Alina Kirillova, Georgi Stoychev, Alla Synytska

Programmed assembly of oppositely charged homogeneously decorated and Janus particles

Erstveröffentlichung in / First published in:

Faraday Discussions. 2016, (191), S. 89–104 [Zugriff am: 01.11.2019]. Royal Society of Chemistry. ISSN 1364-5498.

DOI: https://doi.org/10.1039/c6fd00008h

Faraday Discussions

Cite this: *Faraday Discuss.*, 2016, **191**, 89

PAPER

Programmed assembly of oppositely charged homogeneously decorated and Janus particles†

Alina Kirillova,[ab] Georgi Stoychev[ab] and Alla Synytska*[ab]

Received 29th January 2016, Accepted 11th March 2016
DOI: 10.1039/c6fd00008h

The exploitation of colloidal building blocks with morphological and functional anisotropy facilitates the generation of complex structures with unique properties, which are not exhibited by isotropic particle assemblies. Herein, we demonstrate an easy and scalable bottom-up approach for the programmed assembly of hairy oppositely charged homogeneously decorated and Janus particles based on electrostatic interactions mediated by polyelectrolytes grafted onto their surface. Two different assembly routes are proposed depending on the target structures: raspberry-like/half-raspberry-like or dumbbell-like micro-clusters. Ultimately, stable symmetric and asymmetric micro-structures could be obtained in a well-controlled manner for the homogeneous–homogeneous and homogeneous–Janus particle assemblies, respectively. The spatially separated functionalities of the asymmetric Janus particle-based micro-clusters allow their further assembly into complex hierarchical constructs, which may potentially lead to the design of materials with tailored plasmonics and optical properties.

1. Introduction

Self-assembly is a process where individual building blocks form higher-ordered, organized structures as a consequence of specific, local interactions among the components themselves, in the absence of external guidance.[1] Colloidal particles, which can be synthesized with unprecedented control over their geometry and interactions, may be considered as programmed building blocks for the rational design of functional materials, analogous to atoms being the building blocks for molecules, macromolecules, and crystals.[2] Therefore, colloidal self-assembly represents not only an important model system to study the atomic world,[3] but also a powerful tool for the development of materials with tunable and multi-functional properties.[4–10] Colloidal structures prepared through self-assembly are

[a]*Leibniz Institute of Polymer Research Dresden, Hohe Str. 6, 01069 Dresden, Germany. E-mail: synytska@ipfdd.de*
[b]*Technische Universität Dresden, Fakultät Mathematik und Naturwissenschaften, 01062 Dresden, Germany*
† Electronic supplementary information (ESI) available. See DOI: 10.1039/c6fd00008h

interesting themselves from the theoretical point of view,[11–15] and additionally have a broad variety of potential applications in, for example, photonic/plasmonic devices, photovoltaics, nanoscale electronics, high efficiency energy-conversion/energy-storage, miniature diagnostic systems, drug/gene delivery, and hierarchically structured catalysts.[3,16–18]

The self-assembly process of colloidal particles can be governed by different forces including van der Waals, electrostatic, hydrogen bonding, covalent, coordination, capillary, convective, shear, optical, and electromagnetic forces.[3,19,20] In particular, electrostatic interactions between the particles can be utilized to direct the formation of specially assembled structures.[21–24] The strength of the electrostatic interactions can be tuned continuously by screening the charges and by changing the properties of the medium,[25] and therefore, such interactions can be used to fabricate responsive functional materials.

The aforementioned examples concern the utilization of isotropic colloidal building blocks and their assembly into symmetrical structures. However, the addition of asymmetry at the building block level can facilitate the assembly of such anisotropic building blocks into structures with unique properties, which are not exhibited by isotropic particle assemblies.[11,26–32] For instance, it was suggested that patchy colloids can be used to assemble a diamond lattice of colloidal particles, which provides a larger photonic band gap than many other structures, and thus may be of great use for optoelectronic devices or display applications.[13] Nonetheless, the programmed fabrication of asymmetric structures remains a challenge. Difficulties arise particularly when trying to achieve both spatial and chemical control over the assembly process, which can result in a limited yield, and thus limited applications of the prepared nanomaterials. One direction worth exploring in this context is the creation of a specially designed microscale platform with well-defined spatially separated functionalizations for further use in generating asymmetric assembled structures.

Janus particles (named after the two-faced Roman god) represent a class of multifunctional particles, comprising two different functions on their opposite sides. Their unique anisotropic properties and resemblance to molecular amphiphiles, such as surfactants, phospholipids, and block copolymers, have attracted significant attention in recent years.[33] Due to their multifunctional character, Janus particles have found their applications in a variety of research fields, including stabilization of emulsions,[34–36] chemical catalysis,[37,38] drug delivery,[39] display technology,[40,41] *etc.* Progress has also been made in the area of Janus particle assembly by taking advantage of their asymmetric structure.[34,42–47] However, Janus–Janus particle assembly is typically the focus of the investigations, leaving out the potentially very interesting combination of homogeneous–Janus particles. For instance, a DNA-directed approach was reported for the assembly of asymmetric nanoclusters on a prefabricated Janus particle platform, yielding nanostructures with tunable optical properties.[27] Moreover, the assembly of a binary colloidal system further extends the possibilities to construct complex structures, as colloidal clusters of identical spheres possess limited flexibility in that sense. It was suggested that it is almost impossible to assemble novel colloidal crystals using colloidal clusters of all identical spheres as building blocks.[31,48]

Herein, we report an easy and scalable bottom-up approach for the programmed assembly of binary mixtures of oppositely charged colloidal particles

with hairy polymer shells into specially designed target structures: raspberry-like and dumbbell-like micro-clusters. Two different kinds of assemblies are explored in this context: homogeneous–homogeneous particles, and homogeneous–Janus particles, both of which are based on electrostatic interactions mediated by polyelectrolytes on the surface of the particles. The homogeneous particles serve as a platform for generating symmetric structures, while the Janus particles take part in generating asymmetric structures. The obtained results represent a generalized assembly route for the engineering of tunable micro-cluster architectures from the bottom up, which can be further treated as "colloidal molecules" to assemble even more complex hierarchical materials.

2. Experimental section

Materials

Tetraethylorthosilicate (TEOS, Fluka, 99%), ammonium hydroxide (NH_4OH, Acros Organics, 28–30% solution), ethanol abs. (EtOH, VWR, 99.9%), 3-aminopropyltriethoxysilane (APS, ABCR, 97%), α-bromoisobutyryl bromide (Aldrich, 98%), α-bromoisobutyric acid (Aldrich, 98%), anhydrous dichloromethane (Acros Organics, 99.8%), triethylamine (99%, Sigma-Aldrich), fluorescein *o*-acrylate (Aldrich, 97%), rhodamine B isothiocyanate (mixed isomers, BioReagent, Aldrich), copper(II) bromide (Aldrich, 99.999%), tin(II) 2-ethylhexanoate (Aldrich, 95%), tris(2-pyridylmethyl)amine (TPMA, Aldrich, 98%), *N*,*N*,*N*′,*N*″,*N*″-pentamethyldiethylenetriamine (PMDTA, Aldrich, 99%), anhydrous *N*,*N*-dimethylformamide (DMF, Sigma-Aldrich, 99.8%), ethyl α-bromoisobutyrate (EBiB, Aldrich, 98%), toluene (Sigma-Aldrich, 99.8%), chloroform (Sigma-Aldrich, 99.5%), hydrochloric acid (Sigma, 36.5–38.0%), methanesulfonic acid (Sigma-Aldrich, 99.5%), sodium hydroxide (pellets, Sigma-Aldrich, 97%), diethyl ether (Aldrich, 99.7%), paraffin wax (mp 53–57 °C, Aldrich), *N*-(3-dimethylaminopropyl)-*N*′-ethylcarbodiimide hydrochloride (EDC, Sigma-Aldrich), *N*-hydroxysuccinimide (NHS, Aldrich, 98%), dichloromethane (Acros Organics, 99.99%), hexane (Sigma-Aldrich, 95%), and carboxy terminated poly(lauryl methacrylate) (PLMA, M_n: 11 000 g mol^{-1}; Polymer Source) were used as received. *tert*-Butyl acrylate (*t*BA, Aldrich, 98%) and 2-(dimethylamino)ethyl methacrylate (DMAEMA, Aldrich, 98%) were passed through basic, neutral, and acidic aluminum oxides prior to the polymerization. Millipore water was obtained from Milli-Q (Millipore, conductivity: 0.055 μS cm^{-1}).

Scanning electron microscopy (SEM)

All scanning electron microscopy (SEM) images were acquired using a NEON 40 EsB CrossBeam scanning electron microscope from Carl Zeiss NTS GmbH, operating at 3 keV in the secondary electron mode. In order to enhance the electron density contrast, samples were coated with platinum (3.5 nm) using a Leica EM SCD500 sputter coater.

Transmission electron microscopy (TEM) and cryo-TEM

Transmission electron microscopy (TEM) and cryo-TEM images were taken with a Libra 120 TEM from Carl Zeiss NTS GmbH equipped with a LaB_6 source. The acceleration voltage was 120 kV, and an energy filter with an energy window of

15 eV was used. Samples for TEM were prepared by immersing a TEM grid into the dispersion with the respective particles for 20 s and removing excess liquid afterwards with filter paper. Gold grids with a carbon film (300 mesh, CF300-Au-50) were used for the analysis (Electron Microscopy Sciences, USA). The PAA-100 and PDMAEMA/NH_2-JP-200 samples for cryo-TEM were prepared as follows: particles were dispersed in water (0.5 mg ml^{-1}) by sonication for 20 min; the dispersion was adjusted to the desired pH value. Prior to the analysis, 3.5 μl of the sample were taken, blotted and vitrified in liquid ethane at −178 °C. Ultimately, an approximately 200 nm thick ice film was examined using TEM.

Dynamic light scattering (DLS) measurements

A Zetasizer Nano ZS (Malvern Instruments, UK) was used for the determination of the particle size (hydrodynamic diameter) using plastic cells for aqueous suspensions. The device is equipped with a 633 nm laser and with non-invasive backscatter (NIBS) technology to increase the particle size sensitivity.

Electrokinetic measurements

The pH-dependent electrokinetic (zeta potential) measurements of the particles in suspension were carried out using a Zetasizer Nano ZS (Malvern Instruments, UK) and an MPT-2 autotitrator. For all the measurements, the particles were suspended in a 10^{-3} M KCl solution in water. The pH of the prepared suspensions was controlled by adding 0.1 M KOH or HCl aqueous solutions. Three measurements were recorded for each sample at each pH value.

Fluorescence microscopy

Fluorescence microscopy images were obtained using an Axio Imager.A1m microscope with a 100× oil immersion objective (Carl Zeiss Microscopy GmbH, Germany) equipped with a mercury lamp. For data acquisition, a standard FITC (exciter: D480/30x; dichroic: 505DCLP; emitter: D535/40m; Chroma Technology Corp., USA), or TRITC (exciter: D540/25x; dichroic: 565DCLP; emitter: D605/55m; Chroma Technology Corp., USA) filter set in conjunction with a Photometrics Cascade II: 512 camera (Visitron Systems GmbH, Germany) and a MetaMorph imaging system (Universal Imaging, USA) was used.

Thermogravimetric analysis (TGA) and gel permeation chromatography (GPC)

Thermogravimetric analysis was performed to measure the polymer layer thickness on the particle surface. All measurements were conducted in the air atmosphere on a TGA Q 5000IR analyzer (TA Instruments, USA). The molecular weight of the bulk polymers obtained after precipitation was determined using GPC (Gradient HPLC HP Series 1100, Agilent Technologies Inc., USA). The thickness of the grafted layer on the SiO_2 particles as well as the grafting density of the attached polymer chains were determined by the equations described elsewhere.[49] The grafting density of the polymer chains on the particle surface was 0.2–0.3 chains per nm^2.

Synthesis of homogeneously decorated hybrid core–shell particles

Synthesis and pre-modification of monodisperse SiO_2 particles. 100–1000 nm silica particles were synthesized using a multistep hydrolysis–condensation procedure of TEOS in an ammonia hydroxide–ethanol solution based on the Stöber approach,[50] and described in ref. 51. In brief, TEOS was added sequentially into a mixture of ethanol and ammonia solution. The particles produced within one step of the synthesis were used as seeds for the next step. Each reaction was carried out by stirring the mixture at 500 rpm overnight at room temperature (starting from the last addition of TEOS). Subsequently, the dispersion with particles of the desired size was separated from the solvent by centrifugation, yielding monodisperse silica spheres. Purified particles were dried in a vacuum oven at 60 °C and then modified with (3-aminopropyl)triethoxysilane (APS) to introduce amino groups onto the surface. This was achieved by stirring the particles for 12 hours in a 5% APS solution in ethanol. The particles were then purified by repeated washing and centrifugation cycles in ethanol, and dried. Afterwards, the ATRP-initiator (α-bromoisobutyryl bromide) was immobilized onto the surface of the dried amino-modified particles. For this purpose, the particles were dispersed in 35 ml of anhydrous dichloromethane, followed by the addition of 1.4 ml of triethylamine and 0.7 ml of α-bromoisobutyryl bromide. The reaction was carried out at room temperature under constant stirring for 2 hours. The modified particles were purified by repeated washing and centrifugation cycles in ethanol, and dried under reduced pressure at 60 °C.

Grafting of PDMAEMA and P*t*BA using surface-initiated ATRP. Poly(2-dimethylaminoethyl methacrylate) (PDMAEMA) was grafted from the 1 μm initiator-modified particles as follows: 3 ml of anhydrous DMF, 48 μl of $CuBr_2$ (0.1 M solution in DMF), 48 μl of PMDTA (0.5 M solution in DMF), 0.15 μl of EBiB, and 3 ml of DMAEMA were added to a test tube containing the initiator-modified silica particles (500 mg) and fluorescein *o*-acrylate (40 mg). The test tube was sealed with a rubber septum and purged with argon. 150 μl of Sn(II) 2-ethylhexanoate were injected. The polymerization was carried out under continuous stirring at 70 °C in a water bath for 2 hours. Particles with the grafted polymer were washed by centrifugation in DMF and ethanol 8 times, and dried under reduced pressure at 60 °C.

A similar procedure was used for the grafting of P*t*BA from the 100, 200, 450, and 600 nm initiator-modified silica particles. Rhodamine B isothiocyanate was added during the preparation of these particles in order to label the resulting PAA-covered particles with a red fluorescent dye. For the polymerization, 7.5 mg of TPMA dissolved in 3 ml of *t*BA, 50 μl of $CuBr_2$ (0.1 M solution in DMF), and 0.15 μl of EBiB were added to the particles. The mixture was sonicated and purged with Ar, followed by the injection of 200 μl of Sn(II) 2-ethylhexanoate. The polymerization was performed under continuous stirring at 115 °C for 2 hours. After the particles were purified by centrifugation and redispersion cycles in toluene and dried, hydrolysis was performed to yield polyacrylic acid (PAA). Briefly, P*t*BA-covered particles were suspended in 5 ml of chloroform in a Teflon centrifuge vial, along with 1 ml of methanesulfonic acid, and the mixture was rapidly stirred for 5 minutes. The modified particles were collected by diluting the mixture with diethyl ether, purified by centrifugation and dried.

Synthesis of hybrid core–shell Janus particles

Preparation of colloidosomes and grafting of the first polymer. Colloidosomes with 1 μm large APS-modified silica spheres were prepared using a wax–water Pickering emulsion approach as described elsewhere.[49,51] The ATRP-initiator (α-bromoisobutyric acid) was then immobilized onto the exposed particle surface.[52] Subsequently, wax was dissolved in hexane, and partly initiator-covered particles were used for polymerization. PDMAEMA was grafted from the modified particle surface in the same manner as described above for the homogeneously decorated particles. Fluorescein *o*-acrylate (2 wt%) was added to the reaction mixture to label the grafted polymer.

Grafting of the second polymer. The "grafting to" approach was utilized to graft the second polymer onto the particles modified in the previous step (PDMAEMA/NH_2-JP). For this purpose, silica particles with the grafted first polymer were dispersed in 20 ml of a 1 wt% carboxy terminated poly(lauryl methacrylate) (PLMA) solution in chloroform, and stirred for 2 hours. Next, the solvent was evaporated and the particles were annealed at 150 °C overnight. The ungrafted polymer chains were removed by multiple redispersion cycles of the particles in appropriate solvents and subsequent centrifugation. As a result, bi-component PDMAEMA/PLMA-JP-1 μm particles were obtained.

Self-assembly experiments

Self-assembly experiments were carried out by mixing different ratios of PAA-covered particles with either PDMAEMA homogeneously decorated particles or PDMAEMA/PLMA Janus particles depending on the target structures: raspberry-like or dumbbell-like micro-clusters. Mass ratios of small-to-big particles used for the preparation of raspberry-like micro-clusters were estimated based on the ratio of the big particle surface area to the area of the small particle projections on the surface of a big particle. The ratios were then varied in order to experimentally obtain the dumbbell-like micro-clusters.

For a typical experiment, 1 mg ml^{-1} dispersions of particles of all sizes were prepared in DI water; the pH was adjusted to 7 in each of them. All the dispersions were kept for an hour in an ultrasonic bath. Then the particles were mixed in the appropriate ratios by taking aliquots from the initial 1 mg ml^{-1} dispersions depending on the target structures. For the raspberry-like micro-clusters, the dispersion with central PDMAEMA homogeneously decorated particles (HP) or PDMAEMA/PLMA Janus particles (JP) was slowly added dropwise to the dispersion of PAA-covered surrounding particles under continuous stirring. *Vice versa*, for the dumbbell-like micro-clusters, the dispersion of PAA-covered particles was slowly added dropwise to the dispersion of PDMAEMA-HP or PDMAEMA/PLMA-JP. The resulting mixtures were sonicated for 10 minutes, and then stirred at 700 rpm for two hours. Samples for SEM imaging were taken at this point. In order to obtain individual micro-clusters, the mixtures were diluted 5 times, sonicated for 10 more minutes and left to settle overnight. Samples for SEM imaging were then taken from the upper layer of the dispersion. A complete overview of the prepared samples using different small-to-big particle ratios is displayed in Table 1. At least five different dispersions were prepared for each of the particle sizes and mass ratios, and analysed by SEM in order to assess the reproducibility of the results.

Table 1 Overview of the particle mixtures prepared for the self-assembly experiments

PAA-covered particle size, nm	Mass ratio PAA : PDMAEMA-HP				Mass ratio PAA : PDMAEMA/PLMA-JP	
100	2 : 1	1 : 1	1 : 2	1 : 20	2 : 1	1 : 20
200	2 : 1	1 : 1	1 : 10	1 : 100	2 : 1	1 : 10
450	4 : 1	2 : 1	1 : 5	1 : 50	4 : 1	1 : 5
600	6 : 1	3 : 1	1 : 3.3	1 : 33	6 : 1	1 : 5

3. Results and discussion

Synthesis and characterization of the core–shell homogeneous and Janus particles

Oppositely charged core–shell particles homogeneously decorated with either negatively charged poly(acrylic acid) (PAA), or positively charged poly(2-dimethylaminoethyl methacrylate) (PDMAEMA) were fabricated by grafting the respective polymers from a silica core. The diameter of the PDMAEMA-decorated particles was 1 μm, while the diameters of the PAA-decorated particles varied from 100 to 600 nm (Table 2). Partly positively charged/amphiphilic 1 μm hybrid hairy Janus particles were synthesized through a combination of the "grafting from" and "grafting to" approaches,[49,51,52] and comprised a silica core with PDMAEMA and poly(lauryl methacrylate) (PLMA) polymer shells on the opposite sides of the core.

The fabricated particles were further characterized using SEM and TEM. TEM images revealed the core–shell structure of the PAA and PDMAEMA homogeneously decorated particles as well as the Janus particles (Fig. S1†). A complete overview of the particle samples with their exact diameters obtained from the SEM images as well as the thicknesses of the grafted polymer shells obtained from the TEM images is displayed in Table 2. Additionally, SEM images of the fabricated Janus particles revealed their Janus character (Fig. S2†). The estimated Janus ratio of the particles is 2 : 1 (PDMAEMA : PLMA).

The zeta potential of the polymer-decorated particles as a function of pH was determined by measuring their electrophoretic mobility (Fig. S3†). The surface charge on the particles functionalized with acidic (in the case of PAA) or basic

Table 2 List of the synthesized core–shell homogeneous and Janus particles, their diameters (*D*), and polymer shell thicknesses (*H*)

Sample ID	D^{core} (SEM), nm	$D^{core+shell}$ (SEM), nm	*H* (TEM), nm
PAA-100	100 ± 10	145 ± 10	9 ± 2
PAA-200	216 ± 12	244 ± 7	10 ± 2
PAA-450	460 ± 15	491 ± 5	14 ± 3
PAA-600	570 ± 22	590 ± 14	12 ± 3
PDMAEMA-1 μm	920 ± 20	950 ± 20	17 ± 5
PDMAEMA/PLMA-JP-1 μm	920 ± 20	945 ± 24	8 ± 2 (PDMAEMA)

(in the case of PDMAEMA) surface groups is highly dependent on the pH of the dispersion. An increase in the negative zeta potential with increasing pH in the case of the PAA-decorated particles is due to the increased dissociation of acidic surface groups (Fig. S3,† red circles); the isoelectric point (IEP) of these particles is at pH < 2. In the case of the basic amino groups on the PDMAEMA-decorated particles, the number of positively charged groups increases with decreasing pH due to their protonation (Fig. S3,† black circles); the IEP of these particles is at pH 9.9. When the PDMAEMA polymer on the PDMAEMA-decorated particles is quaternized (through the addition of iodomethane), the particles become permanently positively charged: their surface charge becomes independent from the pH value of the dispersion (Fig. S3,† green circles). No IEP is observed in this case up to pH 10. The zeta potential curve corresponding to the Janus particles decorated with positively charged hydrophilic PDMAEMA and uncharged hydrophobic PLMA (Fig. S3,† blue circles) is similar to the PDMAEMA-decorated particle curve due to the swelling of PDMAEMA. However, there is a shift in the IEP from pH 9.9 to 8.2 due to the presence of the hydrophobic uncharged PLMA (the IEP value of PLMA-functionalized particles is around pH 4). This indicates that both polymers are present on the Janus particle surface.[52]

Next, the pH-responsive swelling behaviour of the PAA and PDMAEMA polymers grafted onto the silica particles was evaluated using cryo-TEM (Fig. 1). For this purpose, particles with a 100 nm diameter homogeneously decorated with PAA (PAA-100-HP) as well as Janus particles with a 200 nm diameter partly decorated with PDMAEMA (PDMAEMA/NH_2-200-JP) were investigated under different pH values of the media. As expected, the two polymers demonstrated opposite swelling behaviour. The PAA polymer chains on the PAA-100-HP particles are in a highly swollen and stretched out state at pH 10, intermediately swollen at pH 7, and collapsed at pH 2 (Fig. 1a). On the contrary, the PDMAEMA polymer chains are highly swollen and stretched out at pH 2, intermediately swollen at pH 7, and collapsed at pH 10 (Fig. 1b). At pH 7 both of the polymers are charged and swollen at the same time, therefore, this pH value was used during the self-assembly experiments. The thicknesses of the polymer shells at different pH values were evaluated after statistical analysis of the corresponding TEM images. The quantified swelling behaviour of PAA and PDMAEMA as well as their swelling grades under different conditions are given in Table 3.

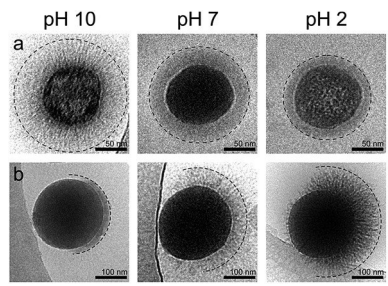

Fig. 1 pH-Responsive behaviour of the grafted polymers evaluated using cryo-TEM images of (a) homogeneous PAA-100-HP particles, and (b) Janus PDMAEMA/NH_2-200-JP particles at different pH values, revealing an opposite swelling behaviour of the PAA and PDMAEMA polymers.

Additionally, the pH-responsive properties of the PAA and PDMAEMA polymers were evaluated using DLS measurements of the corresponding particles (Fig. S4†). The same tendencies in the swelling behaviour as in the cryo-TEM measurements were observed. The hydrodynamic diameter of the 100 nm PAA-decorated particles increases with increasing pH values (Fig. S4a†), while the hydrodynamic diameter of the 1 μm PDMAEMA-decorated particles decreases with increasing pH values (Fig. S4b†).

Self-assembly experiments

We investigated the self-assembly of the synthesized colloidal homogeneous and Janus particles through electrostatic interactions between the charged polyelectrolytes on the surface of the particles. Two main approaches were pursued during the design of the self-assembly experiments depending on the target structures: raspberry-like (or half-raspberry-like in the case of the Janus particles), and dumbbell-like micro-clusters (Fig. 2). For this purpose, we fabricated three types of particles: particles of different sizes homogeneously decorated with PAA, 1 μm particles homogeneously decorated with PDMAEMA, and 1 μm Janus particles decorated with PDMAEMA and PLMA on opposite sides. Large homogeneously decorated particles served as an isotropic platform (especially in approach 1), while the Janus particles served as an anisotropic platform for selective decoration (Fig. 2). In order to demonstrate the generality of our approach, we applied a similar assembly procedure to the mixtures of particles with different size ratios.

First, we explored the self-assembly behaviour of the homogeneously decorated oppositely charged particles by varying the particle mass ratio $M_{\mathrm{PDMAEMA/PAA}} = m_{\mathrm{PDMAEMA}} : m_{\mathrm{PAA}}$, and the particle size ratio $S_{\mathrm{PDMAEMA/PAA}} = D_{\mathrm{PDMAEMA}} : D_{\mathrm{PAA}}$ (Fig. 3). SEM images in the obtained self-assembly diagram demonstrate a clear tendency of the particles to form raspberry-like structures at higher PAA particle concentrations. As expected, with an increase in the PAA-decorated particle diameter, the number of PAA-decorated particles on each large PDMAEMA-decorated particle decreases. With a decrease in the PAA-decorated particle concentration, a tendency to form dumbbell-like structures takes place. Using the more concentrated as-prepared samples, we could obtain networks of the micro-clusters formed during self-assembly (Fig. 3, low magnification images), whereas upon diluting the samples and leaving the mixtures to settle overnight, individual micro-clusters can be obtained (Fig. 3, high magnification images).

Table 3 pH-Responsive behaviour of the grafted PAA and PDMAEMA polymers evaluated using cryo-TEM measurements

	$H^{\text{cryo-TEM}}$, nm			
System/swelling grade	Dry state	pH 10	pH 7	pH 2
PAA-100-HP	9 ± 2	47 ± 4	27 ± 4	15 ± 2
Swelling grade PAA	—	5.0	3.0	1.7
PDMAEMA/NH_2-200-JP	10 ± 3	14 ± 3	42 ± 8	80 ± 10
Swelling grade PDMAEMA	—	1.4	4.0	8.0

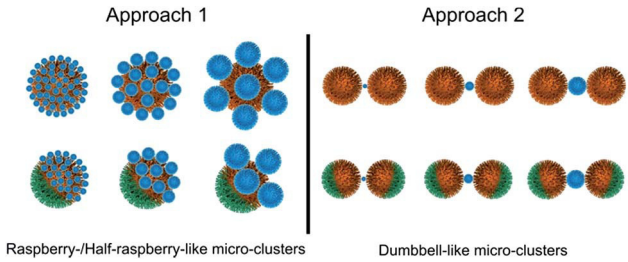

Fig. 2 Proposed schemes for the programmed assembly of homogeneously decorated and Janus core–shell particles in dispersions.

Next, we investigated the self-assembly of homogeneously decorated particles with Janus particles, again, by varying the particle mass ratio $M_{JP/PAA} = m_{JP} : m_{PAA}$, and the particle size ratio $S_{JP/PAA} = D_{JP} : D_{PAA}$ (Fig. 4). The spatially separated regions on a single Janus particle have different chemical properties and surface charges, thus enabling us to assemble asymmetric structures. As a result, half-raspberry-like micro-clusters were formed at higher PAA-decorated particle concentrations, and dumbbell-like micro-clusters were formed at higher Janus particle concentrations (Fig. 4).

Furthermore, we calculated the maximum number of small PAA-decorated particles on a single large (homogeneously decorated or Janus) particle surface. For this purpose, we used the effective diameter of the particles, which was

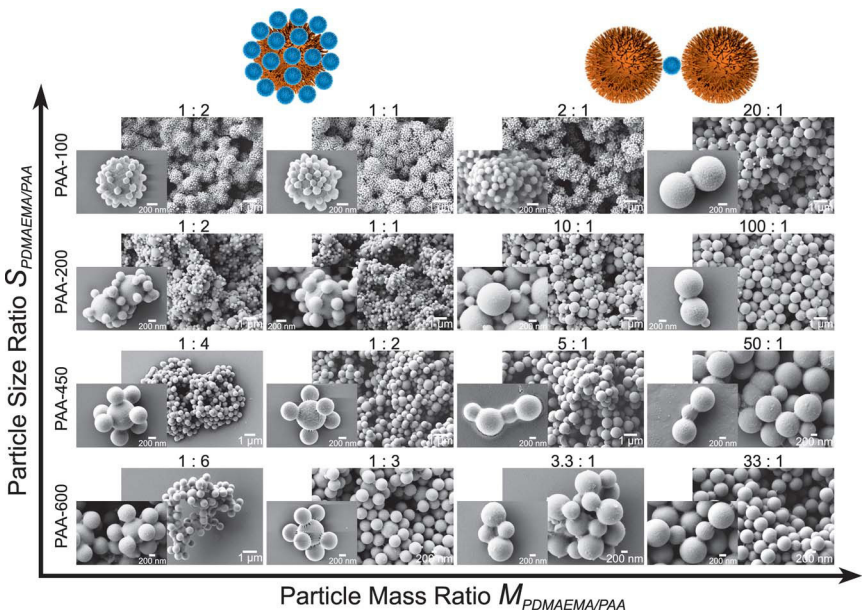

Fig. 3 Diagram with representative SEM images of the structures formed during the self-assembly of particles homogeneously decorated with PAA and PDMAEMA; the particle size ratio $S_{PDMAEMA/PAA}$, and particle mass ratio $M_{PDMAEMA/PAA}$ were varied.

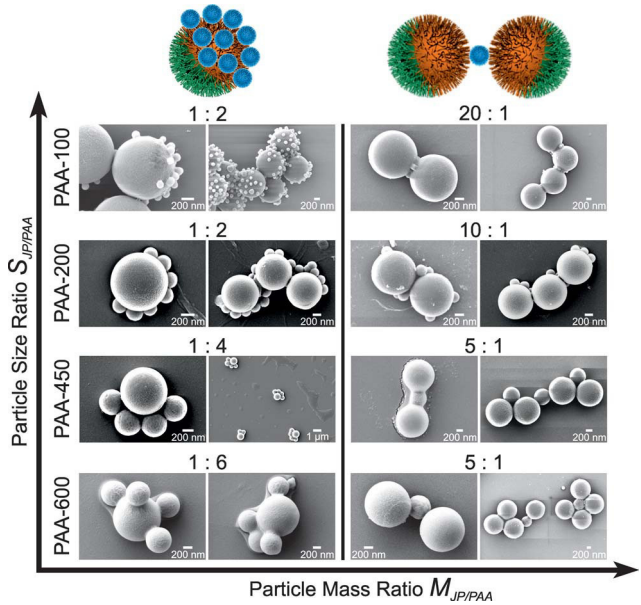

Fig. 4 Diagram with representative SEM images of the micro-clusters formed during the self-assembly of particles homogeneously decorated with PAA and PDMAEMA/PLMA-JP-1 μm; the particle size ratio $S_{JP/PAA}$, and particle mass ratio $M_{JP/PAA}$ were varied.

estimated based on the polymer shell thickness (H) in the dry state and the swelling grade of the respective polymer at pH 7. The results for all the particles are displayed in Table 4. The maximum number of small PAA-covered particles on a single large particle (N) was calculated as previously described in ref. 27, using eqn (1) for the homogeneously decorated large particle (HP), and eqn (2) for the Janus particle (JP), where 2/3 of the particle surface are covered with PDMAEMA (Table 5). Herein, R is the effective radius of the large particle (homogeneously decorated or Janus), whereas r is the effective radius of a PAA-decorated small particle.

$$N = \frac{2}{1 - \frac{\sqrt{R^2 + 2Rr}}{R + r}} \quad (1)$$

Table 4 Particle effective diameters based on the estimated polymer shell thickness in the dry state ($H^{\text{dry state}}$, TEM) and in the swollen state at pH 7 ($H^{\text{swollen state}}$, cryo-TEM)

System	D^{core}, nm	$H^{\text{dry state}}$, nm	$H^{\text{swollen state}}$, nm	$D^{\text{effective}}$, nm
PAA-100	100	9	27	154
PAA-200	216	10	30	276
PAA-450	460	14	42	544
PAA-600	570	12	36	642
PDMAEMA-1 μm	920	17	68	1056
PDMAEMA/PLMA-JP-1 μm	920	8	32	984

Table 5 Theoretical maximum number (N^{theory}) and the experimentally obtained average number ($N^{experiment}$) of the small spheres on a single 1 μm large sphere

	N^{theory}		$N^{experiment}$
PAA system	PDMAEMA-HP	PDMAEMA/PLMA-JP	PDMAEMA/PLMA-JP
PAA-100	246	145	36 ± 13
PAA-200	92	55	7 ± 2
PAA-450	36	20	4 ± 1
PAA-600	27	16	2 ± 1

$$N = \frac{4}{3\left(1 - \frac{\sqrt{R^2 + 2Rr}}{R + r}\right)} \quad (2)$$

We investigated the surface assembly degree by comparing the experimentally obtained number of small particles on the surface of a large Janus particle with the maximum theoretical number (Table 5, Fig. 5). The same trend exists in the experimental results as in the theoretical ones: with increasing the PAA-covered particle size, their number on the surface of a large Janus particle decreases (Fig. 5). However, in the experiments much lower numbers of PAA-covered particles were attached to the PDMAEMA-covered parts of the Janus particles. This can be explained by the fact that PAA-decorated particles randomly attach to the PDMAEMA-covered parts on the Janus particle surface. Unlike in a hexagonal close packing model, such random attachment of the smaller particles leads to large empty spaces between the particles. This is further facilitated by the similar negative charges present on the PAA-covered particles, which act as repulsive forces. Therefore, the particles cannot come near enough to each other to form a close packing model. Statistical analysis of the number of PAA-decorated particles on the surface of a single Janus particle is given in Fig. 6 based on five independent experiments for each particle size ratio. Depending on the

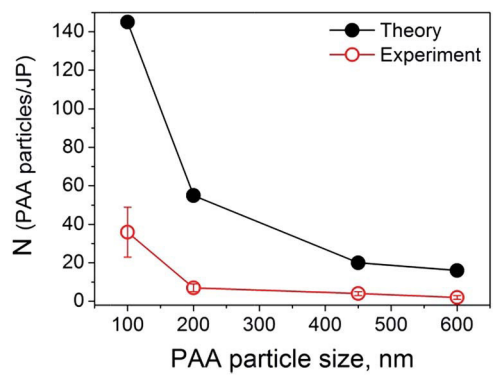

Fig. 5 Comparison of the theoretical and experimental numbers (*N*) of PAA-decorated particles on a single Janus particle depending on the PAA-decorated particle size.

PAA-covered particle size, different numbers of particles are preferentially attached to the Janus particle. A narrow number distribution in the experimental results indicates that the clusters are easily formed in a controlled manner as well as showing very good reproducibility of the results (Fig. 6).

In order to visualize the micro-clusters in dispersion and to exclude the "drying effect" of the SEM imaging, we stained the PAA-covered particles with a red fluorescent dye (rhodamine), and the PDMAEMA shell of the Janus particles with a green fluorescent dye (fluorescein). Three representative examples of the micro-clusters formed in dispersion from PAA-450 homogeneously decorated particles and PDMAEMA/PLMA-JP-1 μm Janus particles at a 4 : 1 ratio are displayed in Fig. 7. Using a standard TRITC filter for imaging, we can see the small PAA-decorated particles, while using a FITC filter the large Janus particles are seen. By combining the two colours, we can observe red-orange spots of PAA-covered particles surrounding the green Janus particle, and forming half-raspberry-like micro-clusters like the ones observed using SEM.

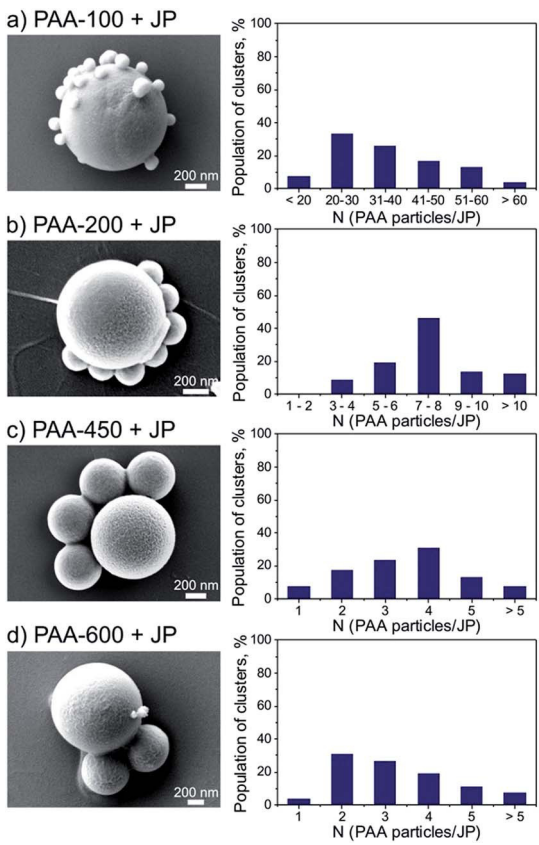

Fig. 6 Representative SEM images of the micro-clusters formed from PAA-decorated particles and PDMAEMA/PLMA-JP, and statistical analysis of the number of PAA-decorated particles on a single Janus particle depending on the PAA-decorated particle size: (a) 100 nm; (b) 200 nm; (c) 450 nm; (d) 600 nm. 200–250 clusters were counted for each particle size ratio (a–d), based on the results from five independent experiments.

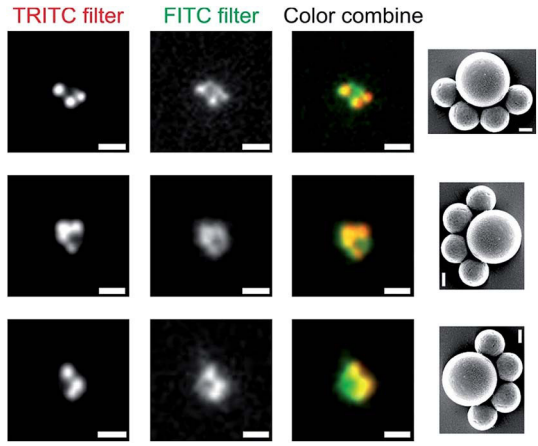

Fig. 7 Fluorescence microscopy images obtained with different filters, and with the colours combined, of the micro-clusters formed in dispersion from PAA-450 homogeneously decorated particles and PDMAEMA/PLMA-JP-1 μm Janus particles (4 : 1). PAA particles adsorb onto one hemisphere of the JPs in the same manner as in the SEM images in the dry state (on the right). Scale bars: 1 μm in the fluorescence microscopy images; 200 nm in the SEM images.

Furthermore, we used cryo-SEM in order to visualize the dumbbell-like structures formed in dispersion from PAA-450 homogeneously decorated particles and PDMAEMA/PLMA-JP-1 μm Janus particles at a 1 : 5 ratio (Fig. S5†). The same micro-clusters as in the dry state were observed in the frozen state (Fig. 4). Additionally, the stability of the assembled structures was investigated by imaging the same dispersions using SEM directly after preparation, and after one week (Fig. S6†). PAA-450 and PDMAEMA/PLMA-JP-1 μm assemblies were chosen as the representative ones for the experiment – both raspberry-like and dumbbell-like structures. The initial dispersions were prepared as described in the Experimental section, and were then left untouched for seven days, after which they were sonicated for 30 minutes. The same micro-clusters were observed in dispersions after 1 week and after additional sonication, which indicates that the structures are perfectly stable in dispersions (Fig. S6,† right panel).

4. Conclusions

Conclusively, we demonstrated an easy and adjustable bottom-up approach for the programmed assembly of hairy oppositely charged colloidal particles: homogeneously decorated particles and Janus particles. Electrostatic interactions between the particles were mediated by polyelectrolytes on their surface, which also introduced pH-responsive properties into the system. We designed two different assembly routes depending on the target structures: raspberry-like (half-raspberry-like) or dumbbell-like micro-clusters. Both homogeneous–homogeneous and homogeneous–Janus particle assemblies were explored in dispersions and in the dry state. Ultimately, stable symmetric and asymmetric micro-structures could be obtained in a well-controlled manner. Moreover, both kinds of particles (homogeneous and Janus) can be easily prepared on a large scale, thus

opening more perspectives for the applications of the assembled micro-clusters. The obtained results therefore represent a generalized assembly route for the large-scale engineering of tunable micro-cluster architectures using the bottom-up approach. Furthermore, the spatially separated functionalities of the asymmetric Janus particle-based micro-clusters allow their further assembly into complex hierarchical constructs, which may potentially lead to the design of materials with tailored plasmonics and optical properties.

Acknowledgements

Deutsche Forschungsgemeinschaft (DFG, Grant SY 125/4-1) and the Leibniz Institute of Polymer Research Dresden (IPF) are acknowledged for financial support. The authors thank Dr Ivan Raguzin for the drawing of the particle 3D pictures.

References

1 S. A. van der Meulen, G. Helms and M. Dogterom, *J. Phys.: Condens. Matter*, 2015, **27**, 233101.
2 Y. Wang, Y. Wang, D. R. Breed, V. N. Manoharan, L. Feng, A. D. Hollingsworth, M. Weck and D. J. Pine, *Nature*, 2012, **491**, 51–55.
3 F. Li, D. P. Josephson and A. Stein, *Angew. Chem.*, 2011, **50**, 360–388.
4 M. H. Lash, J. C. Jordan, L. C. Blevins, M. V. Fedorchak, S. R. Little and J. J. McCarthy, *Angew. Chem.*, 2015, **54**, 5854–5858.
5 H. Y. Koo, D. K. Yi, S. J. Yoo and D. Y. Kim, *Adv. Mater.*, 2004, **16**, 274–277.
6 Y. Cheng, M. Wang, G. Borghs and H. Chen, *Langmuir*, 2011, **27**, 7884–7891.
7 C. M. Liddell and C. J. Summers, *Adv. Mater.*, 2003, **15**, 1715–1719.
8 V. Kitaev and G. A. Ozin, *Adv. Mater.*, 2003, **15**, 75–78.
9 N. Vogel, M. Retsch, C.-A. Fustin, A. del Campo and U. Jonas, *Chem. Rev.*, 2015, **115**, 6265–6311.
10 Y. Wang, Y. Wang, X. Zheng, É. Ducrot, M.-G. Lee, G.-R. Yi, M. Weck and D. J. Pine, *J. Am. Chem. Soc.*, 2015, **137**, 10760–10766.
11 D. Ortiz, K. L. Kohlstedt, T. D. Nguyen and S. C. Glotzer, *Soft Matter*, 2014, **10**, 3541–3552.
12 E. Sanz, M. E. Leunissen, A. Fortini, A. van Blaaderen and M. Dijkstra, *J. Phys. Chem. B*, 2008, **112**, 10861–10872.
13 Z. Zhang, A. S. Keys, T. Chen and S. C. Glotzer, *Langmuir*, 2005, **21**, 11547–11551.
14 Z. Zhang and S. C. Glotzer, *Nano Lett.*, 2004, **4**, 1407–1413.
15 S. Ni, J. Leemann, H. Wolf and L. Isa, *Faraday Discuss.*, 2015, **181**, 225–242.
16 M. Karg, T. A. F. König, M. Retsch, C. Stelling, P. M. Reichstein, T. Honold, M. Thelakkat and A. Fery, *Mater. Today*, 2015, **18**, 185–205.
17 G. A. Ozin, K. Hou, B. V. Lotsch, L. Cademartiri, D. P. Puzzo, F. Scotognella, A. Ghadimi and J. Thomson, *Mater. Today*, 2009, **12**, 12–23.
18 M. Tebbe, M. Mayer, B. A. Glatz, C. Hanske, P. T. Probst, M. B. Muller, M. Karg, M. Chanana, T. A. F. Konig, C. Kuttner and A. Fery, *Faraday Discuss.*, 2015, **181**, 243–260.
19 Z. Mao, H. Xu and D. Wang, *Adv. Funct. Mater.*, 2010, **20**, 1053–1074.
20 Y. Min, M. Akbulut, K. Kristiansen, Y. Golan and J. Israelachvili, *Nat. Mater.*, 2008, **7**, 527–538.

21 M. E. Leunissen, C. G. Christova, A. P. Hynninen, C. P. Royall, A. I. Campbell, A. Imhof, M. Dijkstra, R. van Roij and A. van Blaaderen, *Nature*, 2005, **437**, 235–240.
22 E. V. Shevchenko, D. V. Talapin, N. A. Kotov, S. O'Brien and C. B. Murray, *Nature*, 2006, **439**, 55–59.
23 B. Bharti, G. H. Findenegg and O. D. Velev, *Langmuir*, 2014, **30**, 6577–6587.
24 M. Rasa, A. P. Philipse and J. D. Meeldijk, *J. Colloid Interface Sci.*, 2004, **278**, 115–125.
25 E. Spruijt, H. E. Bakker, T. E. Kodger, J. Sprakel, M. A. Cohen Stuart and J. van der Gucht, *Soft Matter*, 2011, **7**, 8281–8290.
26 A. H. Groschel and A. H. E. Muller, *Nanoscale*, 2015, **7**, 11841–11876.
27 H. Xing, Z. Wang, Z. Xu, N. Y. Wong, Y. Xiang, G. L. Liu and Y. Lu, *ACS Nano*, 2012, **6**, 802–809.
28 S. C. Glotzer and M. J. Solomon, *Nat. Mater.*, 2007, **6**, 557–562.
29 G. R. Yi, D. J. Pine and S. Sacanna, *J. Phys.: Condens. Matter*, 2013, **25**, 193101.
30 A. Perro, E. Duguet, O. Lambert, J. C. Taveau, E. Bourgeat-Lami and S. Ravaine, *Angew. Chem.*, 2009, **48**, 361–365.
31 Y.-S. Cho, G.-R. Yi, J.-M. Lim, S.-H. Kim, V. N. Manoharan, D. J. Pine and S.-M. Yang, *J. Am. Chem. Soc.*, 2005, **127**, 15968–15975.
32 P. Datskos, D. A. Cullen and J. Sharma, *Angew. Chem., Int. Ed.*, 2015, **54**, 9011–9015.
33 A. Walther and A. H. E. Müller, *Chem. Rev.*, 2013, **113**, 5194–5261.
34 S. Jiang, Q. Chen, M. Tripathy, E. Luijten, K. S. Schweizer and S. Granick, *Adv. Mater.*, 2010, **22**, 1060–1071.
35 B. P. Binks and P. D. I. Fletcher, *Langmuir*, 2001, **17**, 4708–4710.
36 A. Walther, M. Hoffmann and A. H. Muller, *Angew. Chem.*, 2008, **47**, 711–714.
37 J. Faria, M. P. Ruiz and D. E. Resasco, *Adv. Synth. Catal.*, 2010, **352**, 2359–2364.
38 A. Kirillova, C. Schliebe, G. Stoychev, A. Jakob, H. Lang and A. Synytska, *ACS Appl. Mater. Interfaces*, 2015, **7**, 21218–21225.
39 S. Hwang and J. Lahann, *Macromol. Rapid Commun.*, 2012, **33**, 1178–1183.
40 J. M. Crowley, N. K. Sheridon and L. Romano, *J. Electrost.*, 2002, **55**, 247–259.
41 T. Nisisako, T. Torii, T. Takahashi and Y. Takizawa, *Adv. Mater.*, 2006, **18**, 1152–1156.
42 Q. Chen, S. C. Bae and S. Granick, *Nature*, 2011, **469**, 381–384.
43 Q. Chen, J. K. Whitmer, S. Jiang, S. C. Bae, E. Luijten and S. Granick, *Science*, 2011, **331**, 199–202.
44 Q. Chen, S. C. Bae and S. Granick, *J. Am. Chem. Soc.*, 2012, **134**, 11080–11083.
45 L. Hong, A. Cacciuto, E. Luijten and S. Granick, *Nano Lett.*, 2006, **6**, 2510–2514.
46 A. A. Shah, B. Schultz, W. Zhang, S. C. Glotzer and M. J. Solomon, *Nat. Mater.*, 2015, **14**, 117–124.
47 M. S. Fernandez, V. R. Misko and F. M. Peeters, *Phys. Rev. E: Stat., Nonlinear, Soft Matter Phys.*, 2015, **92**, 042309.
48 Y. Xia, B. Gates and Z. Y. Li, *Adv. Mater.*, 2001, **13**, 409–413.
49 S. Berger, A. Synytska, L. Ionov, K.-J. Eichhorn and M. Stamm, *Macromolecules*, 2008, **41**, 9669–9676.
50 W. Stöber, A. Fink and E. Bohn, *J. Colloid Interface Sci.*, 1968, **26**, 62–69.
51 S. Berger, L. Ionov and A. Synytska, *Adv. Funct. Mater.*, 2011, **21**, 2338–2344.
52 A. Kirillova, G. Stoychev, L. Ionov and A. Synytska, *Langmuir*, 2014, **30**, 12765–12774.

